LAWRENCE
LIVERMORE
NATIONAL
LABORATORY

LLNL-JRNL-401258

Air Gaps, Size Effect, and Corner-Turning in Ambient LX-17

P. C. Souers, A. Hernandez, C. Cabacungan, L. Fried, R. Garza, K. Glaesemann, L. Lauderbach, S.-B. Liao, P. Vitello

February 12, 2008

Propellants, Explosives, Pyrotechnics

Disclaimer

Air Gaps, Size Effect, and Corner-Turning in Ambient LX-17

P. Clark Souers*, Andrew Hernandez, Chris Cabacungan, Larry Fried, Raul Garza, Kurt Glaesemann, Lisa Lauderbach, Sen-Ben Liao and Peter Vitello

Energetic Materials Center, Lawrence Livermore National Laboratory, Livermore, CA 94550

*Corresponding author; e-mail: souers1@llnl.gov

Abstract

Various ambient measurements are presented for LX-17. The size (diameter) effect has been measured with copper and Lucite confinement, where the failure radii are 4.0 and 6.5 mm, respectively. The air well corner-turn has been measured with an LX-07 booster, and the dead-zone results are comparable to the previous TATB-boosted work. Four double cylinders have been fired, and dead zones appear in all cases. The steel-backed samples are faster than the Lucite-backed samples by 0.6 μs. Bare LX-07 and LX-17 of 12.7 mm-radius were fired with air gaps. Long acceptor regions were used to truly determine if detonation occurred or not. The LX-07 crossed at 10 mm with a slight time delay. Steady state LX-17 crossed at 3.5 mm gap but failed to cross at 4.0 mm. LX-17 with a 12.7 mm run after the booster crossed a 1.5 mm gap but failed to cross 2.5 mm. Timing delays were measured where the detonation crossed the gaps. The Tarantula model is introduced as embedded in 0 reactive flow JWL++ and Linked Cheetah V4, mostly at 4 zones/mm. Tarantula has four pressure regions: off, initiation, failure and detonation. The physical basis of the input parameters is considered.

Keywords: air gaps, corner turning, dead zones, failure diameter, size effect

1 Introduction

LX-17 (TATB 92.5 wt%/kel-F 800 7.5 wt%) is a much-studied slightly non-ideal explosive. Although classic size (diameter) effect work was done for unconfined PBX 9502 (TATB 95 wt%/kel-F 800 5 wt%) by Campbell [1], no such work exists for LX-17, and we consider this most basic measurement here. All measurements in this paper are at room temperature.

We have previously studied dead zone formation in corner-turning of ambient LX-17 using the air-well (or "hockey puck") and double-cylinder geometries [2,3]. The dead zone, which is a region of unreacted explosive, forms just around the right-angle turn and persists in X-ray pictures for up to 6-7 μs after the turn. Two air-well shots were done with a 3 mm-thick steel liner along the inside wall of the air well. All code runs predicted that the shock wave would short circuit through the steel but the shot gave the same result as the bare ones. Further examination showed that the steel had been hollowed out for a pin along the same line as the other pins, so that the "steel" readings are expected to be the same as the bare ones. We wish to reconsider the steel issue here. The double-cylinder was the original geometry in which the dead zones were discovered [4-6], and we found that dead-zones increase in size as the density of the LX-17 increased from 1.87 to 1.91 g/cm^3, probably because the potential hot spots were pressed out.

We had also considered desensitization [7-9], which dead-presses the explosive with a quick low-pressure pulse so that hot spots cannot form later. Although there is agreement that the effect exists, it has not been studied quantitatively. Perhaps the best example is the study by Campbell and Travis on PBX 9404 [8]. Here, a pre-pulse deadened a region so that a later detonation wave died after a distance of travel, much like run-to-detonation in reverse. Fritz and Kennedy suggested that an air cushion can cause a significant pre-pulse, which would connect desensitization with air gaps [10].

To model dead zones with code stability, we introduced the Tarantula model which uses different rate/pressure relations in different pressure regimes. The model used previously used burn fraction/pressure functions [3], but the Piece-Wise Linear Fit does the same with point-by-point input [11]. This was imbedded in both the simple reactive flow model JWL++ [12] and in Linked CheetahV4.0, which is connected to a 2-D hydrocode [13].

The transverse air gap literature has tended to concentrate on the delay caused by the presence of the gap [14,15], but the wedge experiment that used large gaps had no check to see if detonation re-occurred on the far side [14]. A detonation crossing a transverse air gap blows reaction products across at a surprising speed [16-19]. Atomic hydrogen is thought to reach 20 mm/μs [19], and heavier products would cross more slowly according to the square root of their mass. The products then pile up on the opposite face until an initiation pressure is reached. However, the measurement of actual gap widths at which the detonation just crosses does not seem to have been done.

2 Experimental

The size effect cylinders are made of ram-pressed parts that are assembled so that 10 to 12 parts are present in each cylinder. The metal confined cylinders are copper (Cu) with one old tantalum (Ta) shot. An effort is made to have "full-wall" sizes, ie. with the wall thickness $1/5^{th}$ the radius, but it is not always possible. The unconfined assemblies mostly consist of parts inside a thin Lucite (Lu) shell but a few are bare ratesticks lying on a rack. We began with old-fashioned pin rings, with six shorting pins per ring, that measure an average detonation velocity over the last third of the tube. We have also used linear arrays of shorting pins so that the steadiness of the detonation velocity can be better monitored along the cylinder. We found erratic readings with piezoelectric pins on the unconfined rate-sticks and this data has not been included. The manufacturer confirmed that piezoelectric pins are made to be hit head-on and give inexplicable readings when hit transversely [20].

At the end of most cylinders, we also measure the detonation front breakout as it emerges into the air and lights up a small region between the explosive and a glass slide. A slit is placed over the end of the slide and a streak camera measures the light coming out over time. Using the steady state detonation

velocity, we create the detonation lag in mm as a function of the explosive radius. The edge lag is a qualitative measure of the reaction zone length.

The air-well geometry is shown in Figure 1 [2,3]. A hemispherical detonator ignites the booster, which drives a 1.90 g/cm^3 LX-17 main charge. The booster radius has a 19.05 mm radius and the LX-17 radius is 44.45 mm. Previously we used an ultrafine TATB booster but here we switched to 1.876 g/cm^3 LX-07 (HMX 90 wt%/Viton-A 10 wt%) of the same radius. An air well 15 mm deep is built into the part so that the LX-17 can go straight ahead with a the angle Θ at -90^o and other negative values, but also has to turn upward around the corner at pin 2, which is the origin, with Θ = 90^o being the complete turn. The pins turn the corner from the side toward the well at 30.6^o. The pin arrangement is the same, but another pin has been placed in the well against the inner edge half way up. The corner-turning time was obtained by comparing the results of two pins set in the well close to the turn as well as the bottom straight-ahead shown in Figure 1. Average detonation velocities of 7.24, 8.23, 7.50 and 7.58 mm/μs were assumed for TATB, LX-07, LX-17 and PBX 9502 in the direction of these pins. A 0.1 μs lag was assumed at the TATB edge relative to straight ahead.

The double cylinder is shown in Figure 2. Five 12.7 mm-long pellets of 6.35 mm-radius, 1.77-1.78 g/cm^3 LX-14 lead into a 25.4 mm-radius, 50.8 mm-long 1.90 $\pm$0.003 g/cm^3 LX-17 unconfined part. A 6.35 mm-thick plate of either steel or Lucite backs up the LX-17 where the dead zone forms. The LX-14 passes through a hole in the plate. Piezoelectric pins are set along the edges, and we had no problem because the shock does not hit them transversely. This geometry is cheaper to make than the air-well because all parts are pressed, but the straight-ahead path may not work for calibration. (In the machined air-well geometry, the straight-ahead directions are true, unaffected baseline paths.) The straight-ahead pin in the LX-17 was calculated using 7.45-7.50 mm/μs and the HMX pins with 8.5-8.6 mm/μs, with the three points being averaged for the corner-turn time.

The gap shots were made as shown in Figure 3. Ram-pressed pellets of explosive are pressed to 25.4 mm long and 12.7 mm radius. They are glued to a plastic rack so that gaps between pellets are minimized and the air gap to be studied may be set permanently with a thin spacer to $\pm$0.025 mm. Pins are arranged along the side held by another plastic rack. An RP-1 detonator (radius 3.88 mm) is used to directly initiate 1.86 g/cm^3 LX-07, whose detonation crosses the air gap and hits 6 pellets of LX-07. For the 1.90 g/cm^3 LX-17, a Comp B booster was used, which sets off six donor pellets of LX-17. On the other side of the gap, 6 to 8 pellets of LX-17 were used. The long acceptor set was used because earlier experiments measured gap crossing without knowing whether detonation started up again or not. All the LX-07 and most of the LX-17 shots were done with six donor pellets to reach near-steady state. We later fired some LX-17 shots with the Comp B booster and one LX-17 pellet before the gap.

3 Results

The size effect data are listed in Table 1. The error is from the precision given by the various pins, and this standard deviation becomes larger as the radius approaches failure. The adjusted detonation velocities are converted to the nominal 1.90 g/cm^3 using the our empirical relation for small density changes

$$U_S(adjusted) = \left(\frac{1.90}{\rho_o}\right)^{2/3} U_S(measured) \tag{1}$$

where ρ_o is the initial density and U_S is the detonation velocity. The adjusted data is plotted in Figure 4. The average detonation rate, $<\nu>$, in μs^{-1} comes directly from the slope of this data using [21]

$$<\nu> \approx \frac{-D^2}{\partial U_S / \partial(1/R_O)}. \tag{2}$$

We obtain an infinite radius detonation velocity, D, of 7.66 mm/μs. The confined rate is 46 μs^{-1} and the unconfined rate 40 μs^{-1}. The rate is obtained from the straight-line fits shown in the figure. Several shots of small radius failed and two detonated but at low velocity, which we take to be in the failure region. We take the failure radii to be 4.0 mm for copper-confined and 6.5 mm for Lucite-confined.

Table 2 lists the steady states detonation front curvature results. Besides the edge lag, we also describe the curvature with the empirical equation

$$L = AR^2 + BR^8, \tag{3}$$

where L is the lag (mm), R the radius and A and B coefficients. The first term on the right says that the curvature is elliptical over much of the center region. The second term describes increased breakdown of the front near the edge. Both A and B increase as the cylinders get smaller. This may be seen as well for several cases in Figure 5, where is data is un-retouched. As the cylinder shrinks toward failure, the curvatures become ever more ragged with a greater chance of being off-center. In Table 2, we have added some of Hill's unconfined PBX 9502 data for comparison [22]. All of this data is at steady state except for the result obtained after one LX-17 pellet.

Table 3 lists new air-well data and all ambient double-cylinder data, where the X and Y coordinates are listed. The air well data contains the new LX-07-boosted result, which differs only slightly from the usual

TATB booster. In Figure 6, we see that the LX-07 shot shows times slightly slower in the dead zone region but, with the error at $\pm$0.1 μs, we believe that the difference is not significant. This is important because the boosters would be modeled using program burn for LX-07 and reactive flow for TATB, which can show different results in modeling.

The double cylinder break-out times are shown in Figure 7. In the dead zone region, the steel breakout is faster than the Lucite breakout by 0.6 $\pm$ 0.3 μs, and it appears that the steel does speed up corner-turning because of short-circuiting the shock wave through the metal. Two air well shots returned values from a new pin set halfway up the side of the well at 90^{o}. These were: LX-17 with TATB/steel 1.1 μs and LX-07/no steel 2.4 μs. For the 7.5 mm, these give wave velocities of 6.9 and 3.2 mm/μs. Perhaps this is further evidence of the steel effect. The model shows a 2-3 GPa shock wave that slowly turns the corner but does not cause detonation and could cause desensitization.

The measured air gap data is listed for LX-07 in Table 4 with a summary in Table 5. With six lead-in pellets, the detonation has reached near-steady state at the gap and crosses even 10 mm. We use the nominal detonation velocity of 8.64 mm/μs to calculate the time of the start of the gap, which lies 0.79 mm beyond the last pin of the acceptor. This detonation velocity is used to also calculate the expected times with no gap. The measured gap time and the "straight-through" one are subtracted to get the time delay caused by the gap. The LX-17 air gap results are also listed in Tables 4 and 5. With one pellet of LX-17, the detonation crossed a 1.5 mm gap, failed to cross at 2.5 mm and may have failed after running 115 mm after the 2 mm gap. With six pellets, the detonation reached near-steady state so that it crossed at 3.5 mm but failed at 4 mm. To compute the time delay, we need the no-gap detonation velocities. At steady state, we use the measured values here and those from Table 1 to set the error bars. Because the one-pellet case is not at steady state, we take the continuous detonation velocities measured by David Hare with the embedded fiber optic [23]. His values at 1.88 g/cm^3 have been adjusted to 1.90 g/cm^3 using Eq. (1) so we use a velocity of

$$U_S \approx 7.34 + 0.175[1 - exp(-0.0385x)] , \qquad (4)$$

where x is the distance from the end of the booster. This is used to create the no-gap time that is subtracted from the data to get the delay.

4 Modeling with Tarantula

Tarantula is a kinetic package that can be placed in any reactive flow model, which is then connected to a 2-D CALE-type finite element Lagrange code, which is relaxed in an Eulerian manner in specific regions away from where the measurements are taken. Tarantula has works better inside JWL++ [12] than

in Linked Cheetah V4.0 [13, 24]. The kinetic package is best described by the average reaction rate, which is the rate constant times the pressure to whatever power but without the (1-F) term. Figure 8 shows both simple linear and quadratic reaction rates as well as Tarantula. The simple rates start reacting at zero pressure and so have no on/off threshold behavior. Tarantula has four regions. Below 7.5 GPa, nothing happens. From 7.5 to roughly 18 GPa, a low rate turns on slow initiation. At about 18 GPa, this ramps up rapidly toward detonation, which begins at about 32 GPa. In effect, there are two thresholds: the P_o one seen in initiation and the P_1-to-P_2 jump-up to detonation. The use of a multi-zone rate model is not new, and this model is inspired but differs from the 1-D CpeX model of Leiper and Cooper [25, 26].

Tarantula is built on rate functions defined in the four regions as seen here:

$$\begin{aligned}
&\frac{dF}{dt} = 0, \quad P < P_o \\
&\frac{dF}{dt} = G_1 \left[P - P_o\right]^{b1} (1-F), \quad P_o < P < P_1 \\
&\frac{dF}{dt} = G_2 \left[P - P_o\right]^{b2} (1-F), \quad P_1 < P < P_2 \\
&\frac{dF}{dt} = G_3 (1-F)^{1.5}, \quad P > P_2
\end{aligned} \tag{5}$$

where F is the burn fraction, t the time, P is the hydrocode pressure, equal to the actual pressure plus the artificial viscosity. The model is used here in an analytic form but point-by-point programming is also possible. In both cases, there can be discontinuities of the rate between regions, but we recall that the Ignition & Growth reactive flow model has discontinuous rates as a function of burn fraction as well [27]. The detonation region has a constant rate, with (1-F) raised to the power of 1.5 specially to create a straight-line size effect curve for LX-17.

All the constants in Eq. (5) stay mostly the same, and the ones that are changed are b_2 and G_2. First, a copper cylinder of 1.90 g/cc LX-17 of 4 mm-radius and 2.25 mm wall thickness is run. The settings must give steady state detonation at 7.33-7.35 mm/μs. Then, a copper cylinder of 12.7 mm-radius with 2.6 mm wall thickness should give a detonation velocity of 7.54–7.56 mm/μs and a wall velocity of 1.45–1.50 mm/μs after 20 μs. A 3 mm-radius, 1 mm-wall cylinder is supposed to fail, but detonation is often seen at 7.2–7.3 mm/μs. Once these tests are done, we proceed to the air-well and double cylinder problems. It is clear that individual settings can be found that do the 3-mm cylinder failure, air-well or double cylinder, but it is not clear that one setting does all. This is being investigated and an LLL summary report will be issued.

The tests above can only be done at 4 zones/mm and above, although the failure mechanism in Tarantala will function down to 1 zone/mm. Moreover, the constant G_2 changes considerably from 4 to 8 zones/mm but appears to stabilize at higher zoning. Worse yet, the results of the air well and double cylinders depend on the type of booster used. Generally, we use simple JWL++ with either a linear or quadratic rate. With a given zoning, we can turn up the booster rate constant only so far before the model breaks. This means that LX-17-type rate constants must be used in the booster even if it is made of HMX and should have a rate several times higher. On the good side, the rate constant of the booster may be used to fine-tune the output. We have also used program burn in the booster, but this tends to be too weak in pushing Tarantula. The uncertainty in booster modeling makes any decision regarding the presence of desensitization impossible.

The initiation package in Tarantula does not work well at 4 zones/mm but instead leaps to detonation at 15 GPa. By raising the zoning to 20 zones/mm we now have enough resolution to see the small tenths of a μs delay that occurs above 20 GPa. This would seem to be a general problem with reactive flow.

Next, we apply the model to the air gap, where we initially found that the detonation started up on the far side of the LX-17 gap too easily. We discovered that the Lagrange code spalled off the last zone of the donor explosive and sent it like a flyer across the gap. The spalled zone stayed unreacted for 2 mm and started slowly to react thereafter. The impact of this "flyer" on the far face created a high pressure and we felt that a real unburned surface would break up in transit. We then set the zones of the gap to be quasi-Eulerian, which diffused the flyer and gave us agreement with the go-no go data for both the 1 and 6-pellet cases. An Eulerian code should handle this issue easily.

Although Tarantula predicts the go-no go results, it cannot produce the tenths of a μs delays caused by the restarting of the detonation. This is the initiation problem again, and it can only be solved by having finer zoning.

5 Experimental Justification of the Coefficients

The parameters of the Tarantula model come from the fragmentary evidence. The pressure threshold, P_o, is the asymptotic pressure threshold measured in flyer experiments, run-to-detonation and gap tests, which arrive at a value somewhere between 7.5 and 9 GPa for LX-17 [28-35]. The quadratic power of the pressure in the initiation region comes our critical energy, E_{cr}, equation

$$E_{cr} = \frac{(P - P_O)^2 \tau}{\rho_O U_S} \tag{6}$$

used for initiation, where τ is the pulse length.

P_1 is probably at or a little less than the C-J pressure of 26 GPa. It needs to be high enough so that the run-to-detonation time is small. P_2 should be roughly the failure pressure. If we use the rule-of-thumb [36],

$$P_2 \approx \left(\frac{U_S(fail)}{D} \right)^2 P_m^o, \tag{7}$$

we have 7.664 mm/μs for the infinite-radius detonation velocity, D, and about 7.3 mm/μs at failure. The infinite radius spike pressure, P_m^o, is perhaps 36 GPa so that 32 GPa is reasonable for near-failure.

The detonation rate constant , G_3, comes from assuming that the pure detonation rate is pressure-independent so that, from Eq. (2)

$$G_3 = <\nu> \approx \frac{-D^2}{\partial U_S / \partial (1/R_o)}. \tag{8}$$

Because the power of the pressure is zero in the detonation region, the rate constant is also the rate of about 40-50 μs^{-1}.

This analysis can be carried out on other explosives, so that Tarantula could be applied to TNT or HMX. Ideal explosives will have small thresholds, P_o, and corner-turning experiments would show no effect unless they are tiny. Large air gaps would also needed to stop the re-ignition of ideal explosives.

6 Further Gap Analysis

Despite the problems with the model, it does the air gaps fairly well, as long as the gap mesh is relaxed. We have three experimental cases where the detonation crossed the gap and we determined the time delay. Because we measure on the edge of the rate stick, the time delay rises and then declines to a steady state value, which we plot in Figure 9, with the delays obtained from old data [14]. A measurement along the axis should show a delay that slowly climbs to its final value. It appears so far that the delay time increases with the gap width.

Next, we consider the steady-state detonation front curvature for the unconfined, 12.7 mm-radius rate-stick. In Figure 5, we found reasonable agreement between calculation and measurement for a 12.7 mm-

radius bare ratestick. We shall use the parameter A from calculated curves and take advantage of the change in A as the detonation approaches steady state. In Figure 10, we plot the 50%-probable-detonation gap width as a function of the parameter A. The gap width is the average of the largest gap that the detonation crossed and the smallest that caused failure. There are only two data points, but the model confirms the trend, so that measurement of other geometries with different A values is the obvious next step.

In summary, a set of differing experiments has been run on ambient LX-17 and a model constructed that seeks to describe them all. The use of a multi-zone, pressure-dependent reaction rate works for each type of experiment by itself but the use of a single setting for everything remains undecided and possibly too ambitious.

Acknowledgments

This work performed under the auspices of the U.S. Department of Energy by Lawrence Livermore National Laboratory under Contract DE-AC52-07NA27344.

References

[1] A. W. Campbell, Diameter Effect and Failure Diameter of a TATB-Based Explosive, *Propellants, Explosives, Pyrotechnics*, **1984**, *9*, 183-187.

[2] P. Clark Souers, Henry G. Andreski, Charles F. Cook III, Raul Garza, Ron Pastrone, Dan Phillips, Frank Roeske, Peter Vitello and John D. Molitoris, LX-17 Corner Turning, *Propellants, Explosives, Pyrotechnics,* **2004,** *29* , 359.

[3] P. Clark Souers, Henry G. Andreski, Jan Batteux, Brad Bratton, Chris Cabacungan, Charles F. Cook III, Sabrina Fletcher, Raul Garza, Denise Grimsley, Jeff Handly, Andy Hernandez, Pat McMaster, John D. Molitoris, Rick Palmer, Jim Prindiville, John Rodriguez, Dan Schneberk, Bradley Wong, and Peter Vitello, Dead Zones in LX-17 and PBX 9502, *Propellants, Explosives, Pyrotechnics,* **2006**, *31*, 89-97.

[4] M. Cox and A. W. Campbell, Corner-Turning in TATB, *Proceedings Seventh Symposium (International) on Detonation*, Annapolis, MD, 16-19 June, **1981**, pp. 624-633.

[5] M. Held, Corner-Turning Distance and Retonation Radius, *Propellants, Explosives, Pyrotechnics,* **1989,** *14,* 153-161.

[6] M. Held, Corner Turning Research Test, *Propellants, Explosives, Pyrotechnics,* **1996**, *21,* 177-180 .

[7] S. Nie, J. Deng and A. Persson, The Dead-Pressing Phenomenon in an ANFO Explosive, *Propellants, Explosives, Pyrotechnics*, **1993**, *18*, 73-76 .

[8] R. L. Gustavsen, S. A. Sheffield, R. R. Alcon, R. E. Winter, P. Taylor and D. A. Salisbury, Double Shock Initiation of the HMX Based Explosive EDC-37*, Shock Compression of Condensed Matter-2001*, American Institute of Physics, **2002**, pp. 999-1002.

[9] A. W. Campbell and J. R. Travis, The Shock Desensitization of PBX 9404 and Composition B-3, *Proceedings Eighth Symposium (International) on Detonation*, Albuquerque, NM, July 15-19, **1985**, pp. 1057-1067.

[10] J. N. Fritz and J. E. Kennedy. Air Cushion Effect in the Short-Pulse Initiation of Explosives, *Shock Compression of Condensed Matter-1997*. American Institute of Physics, **1998**, pp. 393-396.

[11] Peter Vitello and P. Clark Souers, The Piece Wise Linear Reactive Flow Rate Model, *Shock Compression of Condensed Matter-2005*, M. D. Furnish, M. Elert, T. P. Russell and C. T. White, eds., American Institute of Physics, **2006**, pp. 507-510.

[12] P. Clark Souers, Steve Anderson, Estella McGuire and Peter Vitello, JWL++: A Simple Reactive Flow Code Package for Detonation, *Propellants, Explosives, Pyrotechnics,* **2000,** *25*, 54-58.

[13] L. E. Fried, K. R. Glaesemann, W. M. Howard, P. C. Souers and P. A. Vitello, Cheetah Code, Lawrence Livermore National Laboratory UCRL-CODE-155944 (**2004**).

[14] P. Clark Souers, Stan Ault, Rex Avara, Kerry L. Bahl, Ron Boat, Doug Gidding, LeRoy Green, Jim Janzen, Ron Lee, W. C. Weingart, Ben Wu and Kris Winer, Gap Effects in LX-17, *Propellants, Explosives, Pyrotechnics,* **2006,** *31*, 294-298.

[15] M. Held, Influence of Transverse Air or Inert-Filled Gaps in HE Charges on the Detonation Velocity, *Propellants, Explosives, Pyrotechnics,* **1995,** *20*, 70-73.

[16] B. C. Taylor and L. W. Ervin, Separation of Ignition and Buildup to Detonation in Pressed TNT, *Proceedings Sixth Symposium (International) on Detonation*, Coronado, CA, 24-27 August, **1976**, pp. 3-10.

[17] T. J. Ahrens, C. F. Allen and R. L. Kovach, Explosive Gas Blast: the Expansion of Detonation Products in Vacuum, *J. Appl. Phys.,* **1971***, 42*, 815-829.

[18] N. Lundborg, Front and Mass Velocity at Detonation in Evacuated Chambers*, Proceedings Fourth Symposium (International) on Detonation*, White Oak, MD, 12-15 October, **1965**, pp. 176-178.

[19] J. E. Hay, W. C. Peters and R. W. Watson, Observations of Detonation in a High Vacuum, *Proceedings Fifth Symposium (International) on Detonation*, Pasadena, CA, 18-21 August, **1970**, pp. 559-565.

[20] Jacques Charest, Dynasen Inc, private communication, **2007**.

[21] P. Clark Souers and Peter Vitello, Analytic Model of Reactive Flow, *Propellants, Explosives, Pyrotechnics,* **2005***, 30*, 381-385.

[22] L. G. Hill, J. B. Bdzil and T. D. Aslam, Front Curvature Rate Stick Measurements and Detonation Shock Dynamics Calibration for PBX 9502 over a Wide Temperature Range, *Eleventh International Detonation Symposium*, Snowmass Village, CO, 31 August- 4 September, 1998, pp. 1029-1037.

[23] D. E. Hare, D. R. Goosman, K. Thomas Lorenz and E. L .Lee, Application of the Embedded Fiber Optic Probe in High Explosive Detonation Studies: PBX 9502 and LX-17, *Thirteenth International Detonation Symposium*, Norfolk, VA, July 23-28, **2006**, proceedings to be published; LLRL report UCRL-CONF-222509 (**2006**).

[24] K. R. Glaesemann and L. E. Fried, Recent Advances in Modeling Hugoniots with Cheetah, *Shock Compression of Condensed Matter-2005*, American Institute of Physics, **2006**, pp. 515-518.

[25] G. A. Leiper and J. Cooper, Reaction Rates and the Charge Diameter Effect in Heterogeneous Explosives, *Proceedings Ninth Symposium (International) on Detonation*, Portland, OR, August 28-September 1, **1989**, pp. 197-207.

[26] Graeme Leiper, Ardfeidh Associates, Lentran, United Kingdom, private communication, **2002**.

[27] C. M. Tarver, W. C. Tao and C. G. Lee, Sideways Plate Push Test for Detonating Explosives, *Propellants, Explosives, Pyrotechnics,* **1996***, 21*, 238-246.

[28] LASL Explosive Property Data, T. R. Gibbs and A. Popolato, eds., University of California, Berkeley, **1980**.

[29] R. K. Jackson, L. G. Green, R. H. Barlett, W. W. Hofer, P. E. Kramer, R. S. Lee, E. J. Nidick, Jr., L. L. Shaw and R. C. Weingart, *Proceedings Sixth Symposium (International) on Detonation,* Coronado, CA, August 24-27, **1976**, pp. 755-765.

[30] D. C. Dallman and Jerry Wackerle, Temperature-Dependent Shock Inititation of TATB-Based Explosives, *Proceedings Tenth Symposium (International) on Detonation,* Boston, MA, July 12-16, **1993**, pp. 130-138.

[31]R. L. Gustavsen, S. A. Sheffield, R. R. Alcon, J. W. Forbes, C. M. Tarver and F. Garcia, Embedded Electromagnetic Gauge Measurements and Modeling of Shock Initiation in the TATB Based Explosives LX-17 and PBX 9502, *Shock Compression of Condensed Matter- 2001*, M. D. Furnish, N. N. Thadhani and Y. Horie, American Institute of Physics, **2002**, pp. 1019-1022.

[32] Thomas Lorenz and Tri Tran, Lawrence Livermore Laboratory, private communications, **2004-2005**.

[33] P. E. Kramer, *Performance and Sensitivity Testing of TATB*, Mason & Hanger-Silas Mason Co., Amarillo, TX, report HMSMP-78-59, November, **1978**.

[34] C. A. Honodel, J. R. Humphrey, R. C. Weingart, R. S. Lee and P. Kramer, Shock Initiation of TATB Formulations, *Proceedings Seventh Symposium (International) on Detonation*, Annapolis, MD, June 16-19, **1981**, pp. 425-434.

[35] P. Clark Souers and Peter Vitello, Initiation Pressure Thresholds from Three Sources, *Propellants, Explos., Pyrotech*, to be published.

[36] P. Clark Souers and Peter Vitello, Analytic Model of Reactive Flow, *Propellants, Explosives, Pyrotechnics*, **2005**, *30*, 381-385.

Table 1. Size effect data for metal-confined and unconfined LX-17.

Expl. Density (g/cm^3)	Wall Matl.	Radius (mm)	Measd Detvel (mm/μs)	Inverse Radius (mm^{-1})	Adj. Detvel (mm/μs)	Detvel stdev (mm/μs)	Wall Thick (mm)	Total Length (mm)	Shot No.
LX-17, 1.90 g/cm^3 nominal; confined									
1.908	Cu	25.424	7.629	0.0393	7.608	0.040	5.19	300	432
1.875	Cu	25.421	7.537	0.0393	7.604	0.040	5.18	300	434
1.904	Cu	25.417	7.616	0.0393	7.605	0.040	2.72	300	470
1.917	Cu	25.417	7.656	0.0393	7.611	0.040	2.72	300	523
1.910	Ta	25.415	7.652	0.0393	7.625	0.040	2.72	300	554
1.908	Cu	25.413	7.645	0.0394	7.624	0.040	2.71	300	553
1.913	Cu	12.707	7.591	0.0787	7.557	0.040	1.37	300	453
1.904	Cu	6.365	7.471	0.1571	7.461	0.030	1.34	152	658
1.900	Cu	4.775	7.389	0.2094	7.389	0.038	3.18	254	685
1.902	Cu	3.980	7.343	0.2513	7.338	0.024	2.37	255	705
1.900	Cu	3.175	6.903	0.3150	6.903		3.18	152	676
1.900	Cu	3.195	failed	0.3130			3.15	459	682
1.900	Cu	3.195	failed	0.3130			3.15	280	683
LX-17, unconfined									
1.902	Lu	12.725	7.525	0.0786	7.520	0.058	3.16	101.6	624
1.887	Lu	12.700	7.519	0.0787	7.554	0.011	3.25	330.0	617
1.893	Lu	12.700	7.510	0.0787	7.529	0.016	3.25	330.0	618
1.903	Lu	9.525	7.485	0.1050	7.477	0.026	1.66	254.0	765
1.905	Lu	7.965	7.481	0.1255	7.468	0.047	1.56	253.0	764
1.915	Lu	7.950	7.474	0.1258	7.435	0.010	1.61	203.2	732
1.908	Lu	6.490	7.477	0.1541	7.456	0.053	1.45	248.7	766
1.920	Lu	6.400	7.485	0.1563	7.433	0.029	1.50	152.5	733
1.913	Lu	5.100	7.226	0.1961	7.193	0.083	1.22	152.4	730
1.910	bare	5.560	fail	0.1799	fail		none	254.0	753
1.910	bare	5.060	fail	0.1976	fail		none	254.0	745
1.904	Lu	3.830	fail	0.2611	fail		0.96	153.1	731

Table 2. Measured 1.89-1/91 g/cm^3 LX-17 detonation front curvatures. Hill's PBX 9502 data is included for comparison. One result is transient and the rest are steady state.

			Wall		Edge	Curvature	
	Shot	Radius	Mater-	Thick	Lag	A	B
Expl.	No.	(mm)	ial	(mm)	(mm)	(mm-1)	(mm-7)
Transient, 25.4 mm long pellet							
LX-17		12.7	bare		1.7	0.008	4.5(-10)
Steady State							
9502	Hill	25.0	bare		2.1	0.002	5(-12)
LX-17	627	12.7	Cu	2.6	1.1	0.005	3(-10)
LX-17	617	12.7	Lu	3.3	1.3	0.005	6(-10)
LX-17	618	12.7	Lu	3.3	1.1	0.005	9(-10)
LX-17	765	9.5	Lu	1.6	1.3	0.009	7(-9)
LX-17	761	9.5	bare		0.7	0.003	7(-9)
9502	Hill	9.0	bare		1.0	0.008	9(-9)
LX-17	732	8.0	Lu	1.6	1.0	0.010	2(-8)
LX-17	764	8.0	Lu	1.6	1.5	0.010	5(-8)
LX-17	756	7.3			0.7	0.011	2(-8)
LX-17	766	6.5	Lu	1.5	1.3	0.018	2(-7)
LX-17	733	6.4	Lu	1.5	1.0	0.019	6(-8)
LX-17	658	6.4	Cu	1.3	0.6	0.010	6(-8)
LX-17	754	5.6			0.9	0.015	5(-7)
LX-17	763	5.6	Lu	1.6	1.1	0.019	4(-7)
LX-17	730	5.1	Lu	1.2	1.5?	0.05	NA
9502	Hill	5.0	bare		0.8	0.020	7(-7)
LX-17	685	4.8	Cu	3.2	1.2	0.05?	NA
LX-17	705	4.0	Cu	2.4	0.3	0.02?	NA
LX-17	744	3.2			0.9	0.008	2.5(-7)

Table 3. Corner-turning data for LX-17 with the air-well and double cylinder geometries. An average of previous TATB-boosted air well shots is included for comparison with the LX-07 boosted shot.

			air well with these boosters:			double cylinder with LX-14 booster					
			LX-07	LX-07	ufTATB			Plastic	Plastic	Steel	Steel
X	Y	Angle Θ	time	Angle Θ	time	x	y	#1 time	#2 time	#1 time	#2 time
(mm)	(mm)	(degrees)	(μs)	(degrees)	(μs)	(mm)	(mm)	(μs)	(μs)	(μs)	(μs)
0.00	7.50	79.0	4.13	79.4	3.92	0.00	12.70		2.05	2.33	2.35
2.92	15.00	66.7	3.85	67.0	3.73	0.00	16.67		3.62	3.51	3.55
6.48	15.00	56.3	3.73	56.5	3.62	0.00	20.64	5.77		4.89	4.82
10.03	15.00	47.9	3.73	48.1	3.64	0.00	24.61	5.44	5.41	4.57	5.04
13.59	15.00	47.9	3.73	48.1	3.64	3.18	25.40	5.47	5.05	4.33	4.83
17.15	15.00	41.2	3.92	41.4	3.75	6.35	25.40	5.18	4.81	4.21	4.62
20.70	15.00	36.0	4.07	36.1	4.01	9.53	25.40	4.95	4.67	4.18	4.51
24.26	15.00	31.7	4.36	31.9	4.29	12.70	25.40	4.84	4.63	4.22	4.49
25.40	12.97	27.1	4.28	26.1	4.29	15.88	25.40	4.82	4.67	4.34	4.56
25.40	6.62	14.6	3.95	14.3	3.79	19.05	25.40	4.88	4.78	4.52	4.69
25.40	0.27	0.6	3.61	0.1	3.55	22.23	25.40	5.02	4.95	4.77	4.89
25.40	-6.08	-13.5	3.50	-14.0	3.53	25.40	25.40	5.34	5.31	5.17	5.25
25.40	-12.43	-26.1	3.61	-26.7	3.66	30.00	25.40	5.78	5.78	5.67	5.73
25.40	-18.78	-36.5	3.83	-37.0	3.92	35.00	25.40	6.29	6.29	6.21	6.25
25.40	-25.13	-44.7	4.16	-45.1	4.29	40.00	25.40	6.84	6.85	6.78	6.81
						45.00	25.40	6.80	6.82	6.74	6.79

Table 4. Air gap data for LX-07 and LX-17. The LX-07 has 6 pellets; the LX-17 comes with 1 or 6. Pin positions and times are referenced to the start of the gap.

Gap (mm)	Position (mm)	Time (μs)	Pel-let	Gap (mm)	Position (mm)	Time (μs)	Pel-let	Gap (mm)	Position (mm)	Time (μs)
LX-07			LX-17				LX-17			
2	-63.50	-7.32	1	1.5	-0.79	-0.11	6	3.5	-63.63	-8.44
	-38.10	-4.40			0.00	0.00			-38.17	-5.06
	-12.70	-1.47			2.29	0.37			-12.71	-1.69
	-0.79	-0.09			14.25	2.53			-0.79	-0.10
	0.00	0.00			39.76	5.67			0.00	0.00
	2.79	0.45			65.26	9.04			4.29	0.73
	14.70	1.83			90.74	12.41			16.20	3.50
	40.10	4.72			116.21	15.77			41.65	6.59
	65.50	7.65			141.69	19.16			67.13	9.84
	90.90	10.58	1	2.0	-0.79	-0.10			92.61	13.19
	116.30	13.52			0.00	0.00			118.06	16.58
	141.70	16.45			10.31	1.34			143.51	19.93
5	-63.65	-7.34			15.49	2.28			156.45	21.62
	-38.20	-4.40			26.60	4.75			168.98	23.31
	-12.73	-1.47			52.00	7.66			181.71	25.00
	-0.79	-0.09			77.40	10.98			194.45	26.71
	0.00	0.00			102.80	14.36	6	4.0	-63.73	-8.43
	5.79	0.81			115.50	20.90			-38.24	-5.05
	17.73	2.30	1	2.5	-0.79	-0.11			-12.74	-1.66
	43.20	5.18			3.29	0.56			-0.79	-0.10
	68.67	8.11			15.22	3.21			4.79	0.84
	94.13	11.03	1	3.5	-0.79	-0.11			16.73	3.26
	106.87	12.52			4.29	0.69			42.21	6.77
	119.60	13.98			16.25	3.51	6	5.0	-63.98	-8.52
	132.32	15.44	1	5.0	-0.79	-0.11			-38.44	-5.11
	145.06	16.89			5.79	0.96			-12.86	-1.71
10	-63.63	-7.35			17.71	3.24			-0.79	-0.11
	-38.18	-4.41	6	2.0	-63.50	-8.48			5.79	0.99
	-12.72	-1.48			-38.10	-5.09			17.73	3.25
	-0.79	-0.09			-12.70	-1.70				
	0.00	0.00			-0.79	-0.11				
	10.79	1.53			0.00	0.00				
	22.73	3.00			2.79	0.48				
	48.18	5.85			14.70	2.35				
	73.62	8.77			40.10	5.62				
	99.07	11.69			65.50	9.00				
	111.80	13.16			90.90	12.39				
	124.51	14.62			116.30	15.79				
	137.22	16.10			141.70	19.16				
	149.95	17.54			167.10	22.55				
					192.50	25.93				

Table 5. Summary of air gap time delays and detonation results.

	pellets	gap (mm)	Result	distance f. gap (mm)	final delay (μs)	error (μs)
LX-17	6	1.5	GO	191	0.28	0.05
	1	2.0	GO	140	0.35	0.12
	6	3.5	GO	191	0.88	0.05
	1	2.5	NO GO	143		
	1	3.5	NO GO	144		
	1	5.0	NO GO	145		
	6	4.0	NO GO	195		
	6	5.0	NO GO	196		
LX-07	6	2	GO	140	0.08	0.03
	6	5	GO	140	0.14	0.04
	6	10	GO	140	0.22	0.03

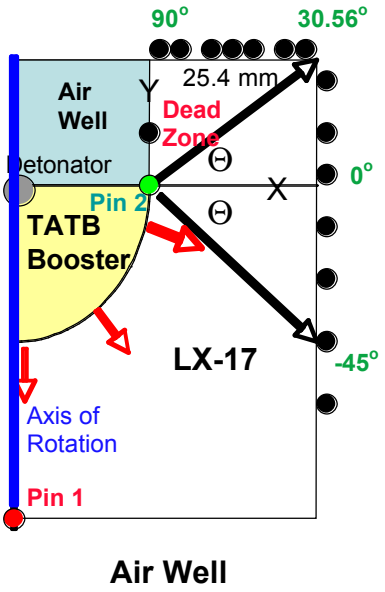

Figure 1. Schematic for the air-well corner-turning experiment. The origin is at pin 2. The black balls are pins.

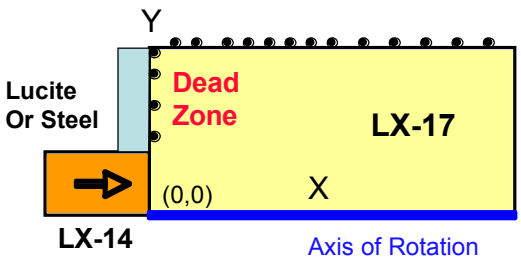

Figure 2. Schematic for the double-cylinder corner-turning experiment. The black balls are pins.

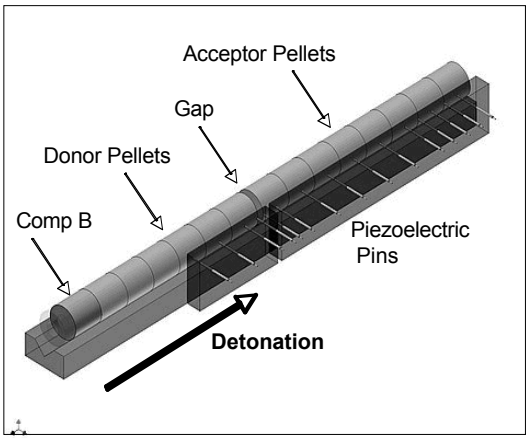

Figure 3. Schematic for the gap experiment. The direction of the detonation is left to right with the gap in the center and pins all along.

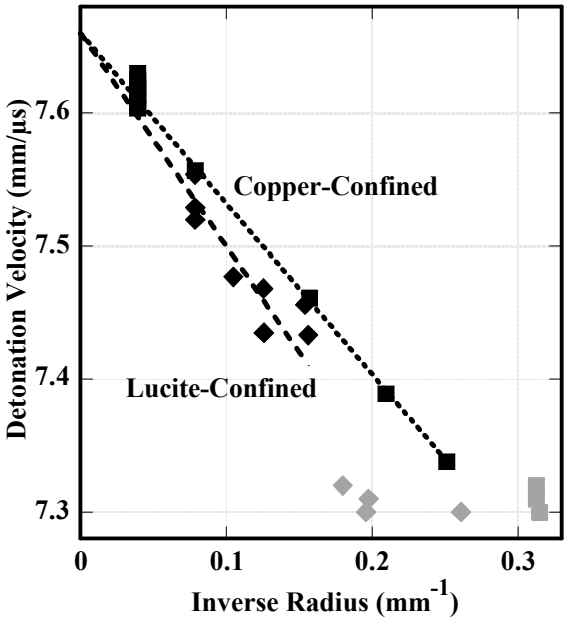

Figure 4. Size (diameter) effect for metal-confined (dark squares) and Lucite-confined (dark diamonds) LX-17 cylinders. The gray symbols are failures. The density-adjusted detonation velocities are plotted.

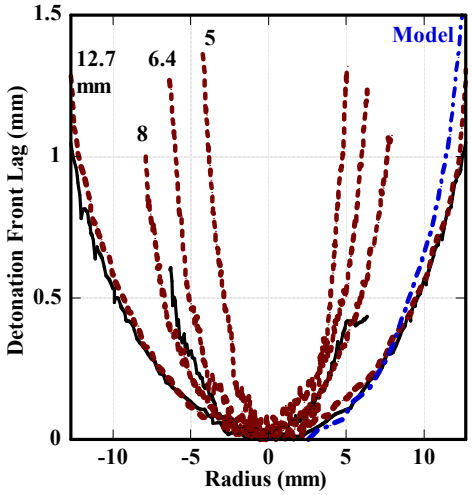

Figure 5. Detonation front curvature for steady state detonation for metal-confined (solid line) and unconfined (Lucite-dashed) LX-17 cylinders of different radii. The model is the dotted line and it agrees with 12.7 mm-radius measurements.

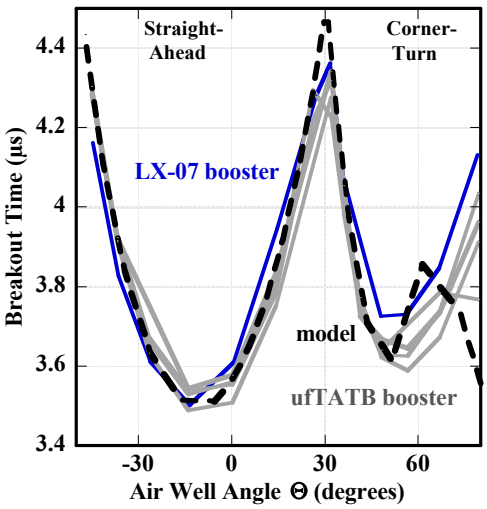

Figure 6. Summary of all air well corner-turning breakout time measurements. The use of an LX-07 booster instead of ultrafine TATB does not matter. The angle Θ is defined in Figure 1: corner-turning sharpness increases as we move left to right.

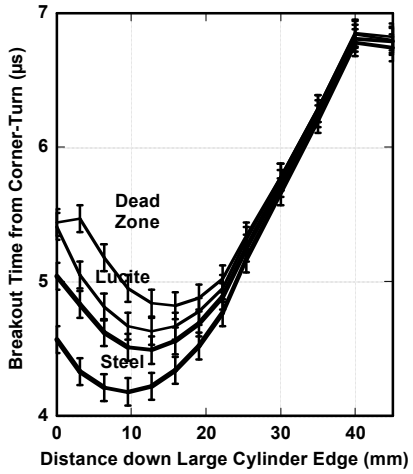

Figure 7. Data for the double cylinder. The steel are the lower two lines and the Lucite the upper two. The distance along the edge is shown in Figure 2.

\

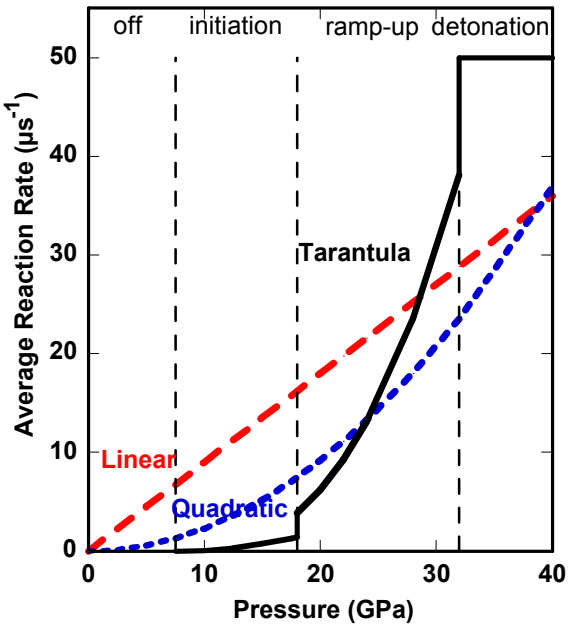

Figure 8. Effective reaction rates for the Tarantula model and the old simple quadratic model (dotted). P_o, P_1 and P_2 mark the transitions between the different pressure regions. Detonation is at the far upper right. No one version of Tarantula matches all the data.

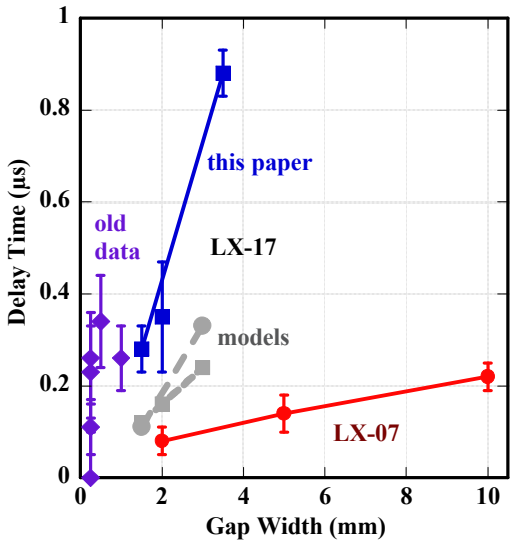

Figure 9. The steady state time delay increases with the gap width and is longer for LX-17 than for LX-07. The calculated delays are too short.

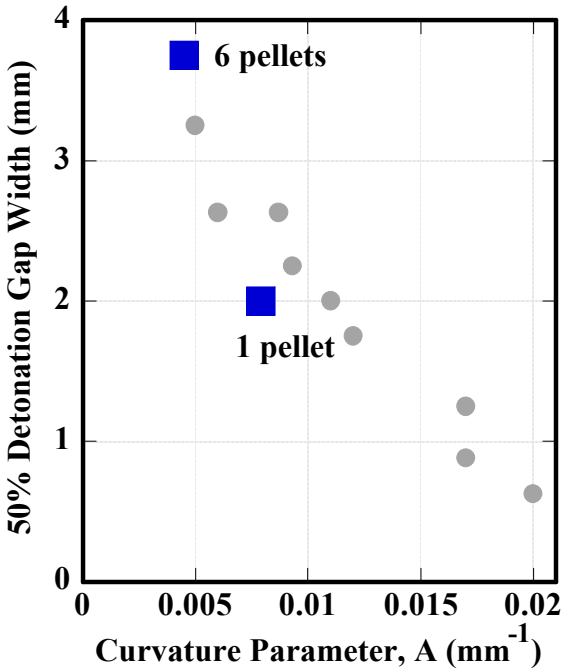

Figure 10. Increase of 50%-probable detonation gap width with decreasing detonation front curvature. The black squares are gap data and the gray circles are calculations.